



# Two-axis gimbal platform controller design in finite time application occasions: LMI approach



Yang Chen <sup>a,b</sup>, Hairong Chu <sup>a,\*</sup>, Tingting Sun <sup>a</sup>, Lihong Guo <sup>a</sup>, Feng Zhang <sup>b</sup>

<sup>a</sup> Changchun Institute of Optics, Fine Mechanics and Physics, Chinese Academy of Sciences, No. 3888, Dongnanhu Rd., Changchun, 130033, Jilin, China

<sup>b</sup> University of Chinese Academy of Sciences, No.19, Yuquan Rd., Beijing 100049, China

## ARTICLE INFO

### Article history:

Received 6 December 2017

Accepted 29 December 2017

### Keywords:

Two-axis gimbal platform

Linear parameter varying state equation

Finite-time boundedness

LMI

## ABSTRACT

In this paper, a controller design approach based on LMI optimization method is proposed for the two-axis gimbal platform in finite time application. This method is based on the linear parameter varying (LPV) model of the two-axis gimbal platform, considering the cross-coupling problem between the pitch and yaw channel. Firstly, the dynamic equation of the two-axis gimbal platform is analyzed and its LPV model is obtained. Then, the sufficient conditions which can ensure the LPV system is finite time bounded(FTB) are introduced, and the controller is designed accordingly. Finally, the performance of the platform with finite time controller and PI controller is analyzed qualitatively. The results show that the proposed controller can guarantee the tracking accuracy in finite time and effectively suppress the coupling interference between the pitch and yaw channel.

© 2017 Elsevier GmbH. All rights reserved.

## 1. Introduction

The payload (such as IR, laser and television) has found a wide use in many important fields, for example guided missiles, tracking systems and image processing. Two-axis gimbal platform controller is used to isolate payload from disturbances. The controller is usually implemented via two loops, the outer loop called track loop and the inner loop called line of sight (LOS) stabilization loop. The typical control architecture of the two-axis gimbal platform is shown in Fig. 1. The track loop consists of specific sensor such as image processor and image tracker. However, in most cases, the LOS stabilization loop employs a two-axis gyro in the inner frame to sense rate disturbance. The LOS stabilization loop determines the performance of the system and is the focus of the design. However, structural defects and cross-coupling between pitch and yaw channels can deteriorate the performance of platform in the condition of the base disturbance [1,2].

Controller design is based on the kinetic model of two-axis gimbal platform, which can be obtained through the Euler rigid body dynamics [3] or Lagrange equation [4]. The configuration of the sensor, which can be divided into direct method and indirect method [5], is another problem of controller design. For most two-axis gimbal platform, direct method is a common approach. After determining the configuration of the sensor, the controller can be designed based on a variety of control methods. So far, several control schemes were introduced to the two-axis gimbal platform design. PID controller and its improved form have been widely used in the controller design [6–8].  $H_\infty$  optimization approach has been regarded as an effective and efficient multivariable robust design method. Compared with the PID controller design procedure, the

\* Corresponding author.

E-mail addresses: [chenyang4688@163.com](mailto:chenyang4688@163.com) (Y. Chen), [chuhr@ciomp.ac.cn](mailto:chuhairong2017@163.com) (H. Chu), [suntt@ciomp.ac.cn](mailto:suntt@ciomp.ac.cn) (T. Sun), [guolh@ciomp.ac.cn](mailto:guolh@ciomp.ac.cn) (L. Guo), [zf00401@163.com](mailto:zf00401@163.com) (F. Zhang).

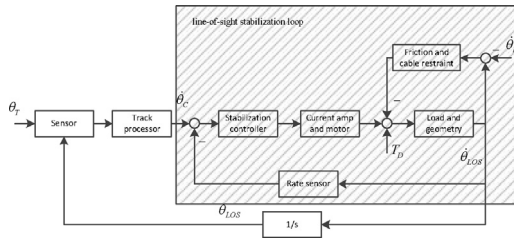


**Fig. 1.** The typical control architecture of the two-axis gimbal platform.

design procedure of  $H_\infty$  can take unmodeled dynamics into consideration and effectively handle the multi-input multi-output(MIMO) systems.  $H_\infty$  control is also widely used in the two-axis gimbal platform [9–11]. Sliding mode control, which is one of the nonlinear robust control methods, has been used in the LOS stabilization loop [12,13]. This method can drive the systems states from any initial state to a user-specified surface. However, the high switching gain and switching action between the different sliding mode surfaces may lead to serious chattering problem [14]. During recent years, some intelligent control strategies, such as adaptive fractional-order sliding-mode [15], fuzzy logical [16,17] and Self-Organizing Recurrent Wavelet-Neural-Network [18] were also applied in LOS stabilization loop.

Sometimes, the two-axis gimbal platform only works for a limited period of time, in which case we only examine its performance during that time period. For example, missile seeker only works in the terminal guidance stage, which begins from the seeker catching a target and ends after the missile hitting the target. This example can be described with finite time stability (FTS) theory. A system is said to be FTS if, given a bound on the initial condition, its state does not exceed a certain threshold during a specified time interval [19]. On this basis, many scholars have studied the finite time stability of various conditions, such as the FTS of continuous systems with additive time-varying delays [20] and FTS for linear discrete-time system with time-varying delay [21]. Amato [22] extended the definition of FTS to the definition of finite-time boundedness (FTB) and provided a sufficient condition guaranteeing FTB via state feedback. For finite-time control problems of linear systems subject to time-varying parametric uncertainties and exogenous disturbance, a synthesis method based on minimizing a linear objective with LMI constraints was presented in [23].

Most of these researches put forward controller based on the model of azimuth axis while the elevation angle was kept fixed, cross moments of inertia were taken to zero and the disturbance from the roll axis of the basement were neglected. When the roll angular velocity of the basement is not zero, the system dynamics and operational conditions will change. So the performance of two-axis gimbal platform with a controller based on single axis model will deteriorate under high dynamic circumstances. To improve control performance, we adopt the LPV model to design the LOS stabilization loop controller in the finite time application. Based on the sufficient condition of FTB, we can get the controller by solving the LMI feasibility problem. When an application environment is determined, we can get more targeted controllers.

The outline of the paper is organized as follows. In Section 2, we establish the dynamic model of the two-axis gimbaled platform and obtained its LPV form. In Section 3, a controller design method based on FTB theory is proposed, and the corresponding parameter setting principle is established. A series of simulations validate the effectiveness of the controller in Section 4. Finally, the conclusions are highlighted in Section 5.

## 2. Dynamic model of a two-axis gimbal platform

### 2.1. Equation of motion of a two-axis gimbal platform

A conventional configuration for the gimbal motion of a two-axis gimbaled platform is depicted as in Fig. 2. Three coordinate frames are used to define the rotation about a dynamic platform, that is a body-fixed frame (B), a frame (A) fixed to the outer yaw (azimuth) gimbal and a frame (E) fixed to the inner pitch (elevation) gimbal.  $x_{az}$   $y_{az}$   $z_{az}$  and  $x_{el}$   $y_{el}$   $z_{el}$  represent the yaw and pitch gimbal frame axis, respectively.  $x_b$   $y_b$   $z_b$  represent the body frame axis. LOS elevation control is exercised via the inner gimbal y-axis, while azimuth control is applied via the outer gimbal z-axis. The angular rate sensors are mounted on the LOS axes. The center of rotation is in the frame origin, which is assumed to be the same point for the three frames.  $\psi$   $\theta$  and  $\phi$  are defined as the Euler angles which uses yaw-pitch-roll transformation order.  $\psi$  represents the relative azimuth angle between the outer and base coordinate frames.  $\theta$  represents the relative elevation angle between the inner and outer coordinate frames.  $\phi$  represents the relative angle between the inertial and base coordinate frames. The transformation matrix can be expressed as below.

$$\mathbf{R}_{z,\psi} = \begin{bmatrix} \cos \psi & \sin \psi & 0 \\ -\sin \psi & \cos \psi & 0 \\ 0 & 0 & 1 \end{bmatrix}, \mathbf{R}_{y,\theta} = \begin{bmatrix} \cos \theta & 0 & -\sin \theta \\ 0 & 1 & 0 \\ \sin \theta & 0 & \cos \theta \end{bmatrix}, \mathbf{R}_{x,\phi} = \begin{bmatrix} 1 & 0 & 0 \\ 0 & \cos \phi & \sin \phi \\ 0 & -\sin \phi & \cos \phi \end{bmatrix} \quad (1)$$

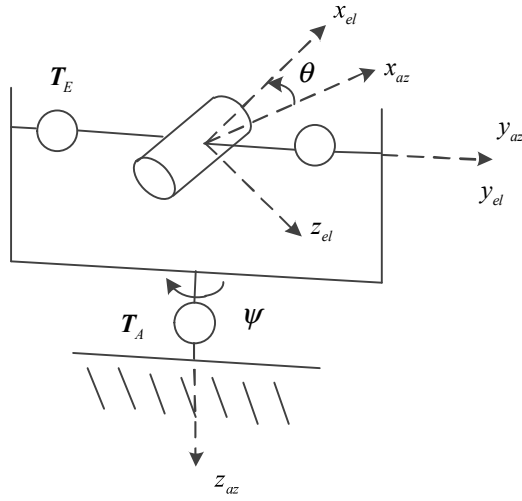


**Fig. 2.** Two-axis gimbaled platform configuration.

We introduce

$$\boldsymbol{\omega}_B = \begin{bmatrix} p \\ q \\ r \end{bmatrix}, \boldsymbol{\omega}_A = \begin{bmatrix} \omega_{ax} \\ \omega_{ay} \\ \omega_{az} \end{bmatrix}, \boldsymbol{\omega}_E = \begin{bmatrix} \omega_{ex} \\ \omega_{ey} \\ \omega_{ez} \end{bmatrix} \quad (2)$$

as the angular velocity vectors of frames B, A and E, respectively. Therefore the angular velocities of the outer and inner gimbal are given by the Euler angular relationship.

$$\boldsymbol{\omega}_A = \mathbf{R}_{z,\psi} \boldsymbol{\omega}_B + [0 \ 0 \ \dot{\psi}]^T \quad (3)$$

$$\boldsymbol{\omega}_E = \mathbf{R}_{y,\theta} \boldsymbol{\omega}_A + [0 \ \dot{\theta} \ 0]^T \quad (4)$$

where  $\dot{\psi} = \omega_{az} - r$  and  $\dot{\theta} = \omega_{ey} - \omega_{ay}$ .

The relationship between the angular acceleration of the inner and outer gimbal coordinate frames is obtained by differentiating (4).

$$\dot{\boldsymbol{\omega}}_E = \mathbf{R}_{y,\theta} \dot{\boldsymbol{\omega}}_A + \dot{\mathbf{R}}_{y,\theta} \boldsymbol{\omega}_A [0 \ \dot{\theta} \ 0]^T + [0 \ \ddot{\theta} \ 0]^T \quad (5)$$

where  $\dot{\mathbf{R}}_{y,\theta} = \begin{bmatrix} -\sin \theta & 0 & -\cos \theta \\ 0 & 0 & 0 \\ \cos \theta & 0 & -\sin \theta \end{bmatrix}$ . Then  $\dot{\boldsymbol{\omega}}_A$  is given by

$$\dot{\boldsymbol{\omega}}_A = \mathbf{R}_{y,\theta}^T \dot{\boldsymbol{\omega}}_E - \mathbf{R}_{y,\theta}^T \dot{\mathbf{R}}_{y,\theta} \boldsymbol{\omega}_A [0 \ \dot{\theta} \ 0]^T - \mathbf{R}_{y,\theta}^T [0 \ \ddot{\theta} \ 0]^T \quad (6)$$

Based on rigid body dynamics, the dynamic equation of motion for a two-axis gimbaled sensor system can be formulated as

$$\mathbf{J}_E \ddot{\boldsymbol{\omega}}_E + \boldsymbol{\omega}_E \times \mathbf{J}_E \boldsymbol{\omega}_E = \mathbf{T}_E \quad (7)$$

where the sum of the kinematic torques about the elevation gimbal is

$$\mathbf{T}_E = \begin{bmatrix} T_{ex} \\ T_{elMotor} \\ T_{ez} \end{bmatrix} - \begin{bmatrix} 0 \\ T_{ef} \\ 0 \end{bmatrix} \quad (8)$$

$T_{ex}$  and  $T_{ez}$  are reaction torques exerted by elevation on azimuth gimbal.  $T_{elMotor}$  is elevation stabilization control torque.  $T_{ef}$  is friction torques. The friction torque consist of both linear and nonlinear parts, so it can be expressed as  $T_{ef} = K_{ef}\dot{\theta} + T_{efric}$ , where  $K_{ef}$  is viscous friction coefficient,  $T_{efric}$  is nonlinear friction torques. To simplify the analysis, it is assumed that the gimbal rotation axes are aligned with the principal axes of inertia so that the inertia sub-matrices of elevation are diagonal  $\mathbf{J}_E = \text{diag}(J_{exx} \ J_{eyy} \ J_{ezz})$ .

The elevation control axis is the inner gimbal y-axis, so the inner gimbal dynamics equation can be expanded as

$$J_{eyy}\dot{\omega}_{ey} = -\omega_{ez}\omega_{ex}(J_{exx} - J_{ezz}) + T_{elMotor} - K_{ef}\dot{\theta} - T_{efric} \quad (9)$$

As the disturbance stems from base rates  $\omega_B$  and the controlled variables are  $\omega_{ey}$  and  $\omega_{ez}$ , so substituting (3) into (4) and then into (9). Then the elevation axis dynamics can be expressed as below

$$J_{eyy}\dot{\omega}_{ey} + K_{ef}\omega_{ey} + \omega_{ez}\left(\frac{\omega_{ax} - \sin\theta\omega_{ez}}{\cos\theta}\right)(J_{exx} - J_{ezz}) = T_{elMotor} - T_{efric} + K_{ef}(q\cos\theta - p\sin\theta) \quad (10)$$

In a similar manner, the torque dynamics for the azimuth gimbal body are derived from

$$\mathbf{J}_A\dot{\boldsymbol{\omega}}_A + \boldsymbol{\omega}_A \times \mathbf{J}_A\boldsymbol{\omega}_A + \mathbf{R}_{y,\theta}^T \mathbf{T}_E = \mathbf{T}_A \quad (11)$$

where  $\mathbf{T}_A = \begin{bmatrix} T_{ax} \\ T_{ay} \\ T_{azMotor} \end{bmatrix} - \begin{bmatrix} 0 \\ 0 \\ T_{af} \end{bmatrix}$ .  $T_{ax}$  and  $T_{ay}$  are azimuth gimbal reaction torques on base.  $T_{azMotor}$  is azimuth stabilization control torque.  $T_{af}$  is the friction torque between base and azimuth gimbal. As with the inner gimbal friction torque.  $T_{af} = K_{af}\dot{\theta} + T_{afric}$ , where  $K_{af}$  is viscous friction coefficient,  $T_{afric}$  is nonlinear friction torques.

Assuming the outer inertia matrix is also diagonal,  $\mathbf{J}_A$  can be expressed as  $\mathbf{J}_A = \text{diag}(J_{axx} \ J_{ayy} \ J_{azz})$ . Substitute the  $\mathbf{T}_E$  as (7) into (11) and the  $\dot{\boldsymbol{\omega}}_A$  as (6) into (10) to obtain

$$\begin{aligned} & [\mathbf{J}_A \mathbf{R}_{y,\theta}^T + \mathbf{R}_{y,\theta}^T \mathbf{J}_E] \dot{\boldsymbol{\omega}}_E + \boldsymbol{\omega}_A \times \mathbf{J}_A \boldsymbol{\omega}_A + \mathbf{R}_{y,\theta}^T (\boldsymbol{\omega}_E \times \mathbf{J}_E \boldsymbol{\omega}_E) \\ & - \mathbf{J}_A \mathbf{R}_{y,\theta}^T \dot{\mathbf{R}}_{y,\theta} \boldsymbol{\omega}_A \begin{bmatrix} \mathbf{0} & \dot{\boldsymbol{\theta}} & \mathbf{0} \end{bmatrix}^T - \mathbf{J}_A \mathbf{R}_{y,\theta}^T \begin{bmatrix} \mathbf{0} & \ddot{\boldsymbol{\theta}} & \mathbf{0} \end{bmatrix}^T = \mathbf{T}_A \end{aligned} \quad (12)$$

The azimuth axis dynamics are generated by the third element of vector (12). Expanding the equation for this component results in

$$\begin{aligned} \bar{J}_{az}\dot{\omega}_{ez} &= \sin\theta(J_{az} + J_{ex})\dot{\omega}_{ax} + (J_{az}\omega_{ez} - \sin\theta J_{ex}\omega_{az})\dot{\theta} \\ & - \cos\theta[\omega_{ax}\omega_{ay}(J_{ay} - J_{ax}) - \sin\theta\omega_{ey}\omega_{ez}J_{ez} + \omega_{ey}\omega_{ax}J_{ey} - \cos\theta\omega_{ex}\omega_{ey}J_{ex}] \\ & + \cos\theta[T_{azMotor} - T_{af} - K_{af}\dot{\theta}] \end{aligned} \quad (13)$$

where  $\bar{J}_{az} = J_{az} + \cos^2\theta J_{ez} + \sin^2\theta J_{ex}$

As with the elevation axis, this equation needs to be expressed in terms of the controlled variables  $\omega_{ez}$   $\omega_{ey}$ , the elevation and azimuth angles  $\theta$  and  $\psi$ , and base disturbances. Based on (3) and (4), we can get

$$\omega_{ex} = \frac{1}{\cos\theta}(\omega_{ax} - \sin\theta\omega_{ez}) \quad (14)$$

$$\omega_{az} = \frac{1}{\cos\theta}(\omega_{ez} - \sin\theta\omega_{ax}) \quad (15)$$

Substitute (14) and (15) into (13), the modified expression is derived as

$$\bar{J}_{az}\dot{\omega}_{ez} = g_z\omega_{ez} + g_y\omega_{ax}\omega_{ey} + g_{yz}\omega_{ey}\omega_{ez} + T_{obase} + \cos\theta[T_{azMotor} - T_{af}] \quad (16)$$

where  $T_{obase}$  is the disturbance from base motion.

$$\begin{aligned} T_{obase} &= (\cos\psi\dot{p} + \sin\psi\dot{q} - \omega_{ay}r)(J_{azz} + J_{exx})\sin\theta \\ & - \frac{1}{\cos\theta}J_{azz}\omega_{ax}\omega_{ay}(1 + \sin^2\theta) - 2J_{exx}\omega_{ax}\omega_{ay}\frac{\sin^2\theta}{\cos\theta} \\ & - (J_{ayy} - J_{axx})\omega_{ax}\omega_{ay}\cos\theta + K_{af}\cos\theta(\sin\theta\omega_{ax} + r) \end{aligned} \quad (17)$$

$$g_y = \frac{1}{\cos\theta}(J_{azz} + \sin^2\theta J_{exx})\omega_{ax} + \cos\theta(J_{exx} - J_{eyy})\omega_{ax} \quad (18)$$

$$g_z = 2\tan\theta(J_{exx} + J_{azz})\omega_{ay} - K_{af} \quad (19)$$

$$g_{yz} = -(J_{azz} + J_{exx}) \tan \theta + (J_{ezz} - J_{exx}) \sin \theta \cos \theta \quad (20)$$

## 2.2. LPV form of the stabilization loop

The elevation and azimuth axis dynamics can be expressed in a state differential equation form as

$$\dot{\mathbf{x}} = \mathbf{A}(t)\mathbf{x} + \mathbf{D}(\mathbf{x}, t) + \mathbf{J}^{-1}(\mathbf{T}_{motor} + \mathbf{T}_{obase} + \mathbf{T}_{nonlinear}) \quad (21)$$

where

$$x_1 = \int_0^t \omega_{ey}(\tau) d\tau; x_2 = \omega_{ey}(t); x_3 = \int_0^t \omega_{ez}(\tau) d\tau; x_4 = \omega_{ez}(t) \quad (22)$$

$$\mathbf{A}(t) = \begin{bmatrix} 0 & 1 & 0 & 0 \\ 0 & -\frac{K_{ef}}{J_{eyy}} & 0 & -\frac{J_{exx} - J_{ezz}}{J_{eyy} \cos \theta} \omega_{ax} \\ 0 & 0 & 0 & 1 \\ 0 & \frac{g_y}{\bar{J}_{az}} & 0 & \frac{g_z}{\bar{J}_{az}} \end{bmatrix} \quad (23)$$

$$\mathbf{D}(\mathbf{x}, t) = \begin{bmatrix} 0 \\ \frac{(J_{exx} - J_{ezz}) \sin \theta}{J_{eyy} \cos \theta} x_4^2 \\ 0 \\ \frac{g_{yz} x_2 x_4}{\bar{J}_{az}} \end{bmatrix} \quad (24)$$

$$\mathbf{J}^{-1} = diag(0, 1/J_{eyy}, 0, 1/\bar{J}_{az}) \quad (25)$$

$$\mathbf{T}_{motor} = [0 \ T_{elMotor} \ 0 \ T_{azMotor}]^T \quad (26)$$

$$\mathbf{T}_{obase} = [0 \ K_{ef} (q \cos \theta - p \sin \theta) \ 0 \ T_{obase}]^T \quad (27)$$

$$\mathbf{T}_{nonlinear} = [0 \ -T_{efric} \ 0 \ -\cos \theta T_{efric}] \quad (28)$$

$\mathbf{D}(\mathbf{x}, t)$  is omitted after linearizing the system at the equilibrium point. System matrix  $\mathbf{A}(t)$  changes according to  $\omega_{ax}(t)$  and  $\omega_{ay}(t)$ , what's more, azimuth and elevation axis dynamics are coupling.

Assuming  $\omega_{ax}(t)$  and  $\omega_{ay}(t)$  are bounded and in the polytope of vertices:

$$\omega_{ax}(t) \in [-\omega_{ax0}, \omega_{ax0}] \quad (29)$$

$$\omega_{ay}(t) \in [-\omega_{ay0}, \omega_{ay0}] \quad (30)$$

The linearized LOS stabilization loop is a polytopic LPV system with exogenous disturbance:

$$\dot{x}(t) = A(p(t))x(t) + Bu(t) + Gw(t) \quad (31)$$

where  $B = G = \mathbf{J}^{-1}$ ,  $u(t) = \mathbf{T}_{motor}$ ,  $w(t) = \mathbf{T}_{obase} + \mathbf{T}_{nonlinear}$ ,  $A(p(t))$  is constrained to the polytope  $\mathbf{P}$  given by

$$\mathbf{P} = \left\{ A(p(t)) : A(p(t)) = \sum_{j=1}^4 p_j(t) A_j, \sum_{j=1}^4 p_j(t) = 1, p_j(t) \geq 0, j = 1, \dots, 4 \right\} \quad (32)$$

and

$$\mathbf{A}_1 = \begin{bmatrix} 0 & 1 & 0 & 0 \\ 0 & -\frac{K_{ef}}{J_{eyy}} & 0 & -\frac{J_{exx} - J_{ezz}}{J_{eyy} \cos \theta} (-\omega_{ax0}) \\ 0 & 0 & 0 & 1 \\ 0 & \frac{g_{y1}}{\bar{J}_{az}} & 0 & \frac{g_{z1}}{\bar{J}_{az}} \end{bmatrix}, \mathbf{A}_2 = \begin{bmatrix} 0 & 1 & 0 & 0 \\ 0 & -\frac{K_{ef}}{J_{eyy}} & 0 & -\frac{J_{exx} - J_{ezz}}{J_{eyy} \cos \theta} (\omega_{ax0}) \\ 0 & 0 & 0 & 1 \\ 0 & \frac{g_{y2}}{\bar{J}_{az}} & 0 & \frac{g_{z2}}{\bar{J}_{az}} \end{bmatrix} \quad (33)$$

$$\mathbf{A}_3 = \begin{bmatrix} 0 & 1 & 0 & 0 \\ 0 & -\frac{K_{ef}}{J_{eyy}} & 0 & -\frac{J_{exx} - J_{ezz}}{J_{eyy} \cos \theta} (-\omega_{ax0}) \\ 0 & 0 & 0 & 1 \\ 0 & \frac{g_{y3}}{\bar{J}_{az}} & 0 & \frac{g_{z3}}{\bar{J}_{az}} \end{bmatrix}, \mathbf{A}_4 = \begin{bmatrix} 0 & 1 & 0 & 0 \\ 0 & -\frac{K_{ef}}{J_{eyy}} & 0 & -\frac{J_{exx} - J_{ezz}}{J_{eyy} \cos \theta} (\omega_{ax0}) \\ 0 & 0 & 0 & 1 \\ 0 & \frac{g_{y4}}{\bar{J}_{az}} & 0 & \frac{g_{z4}}{\bar{J}_{az}} \end{bmatrix}$$

$$g_{y1} = g_{y3} = \frac{1}{\cos \theta} (J_{azz} + \sin^2 \theta J_{exx}) (-\omega_{ax0}) + \cos \theta (J_{exx} - J_{eyy}) (-\omega_{ax0}) \quad (34)$$

$$g_{z1} = g_{z2} = 2 \tan \theta (J_{exx} + J_{azz}) (-\omega_{ay0}) - K_{af}$$

$$g_{y2} = g_{y4} = \frac{1}{\cos \theta} (J_{azz} + \sin^2 \theta J_{exx}) (\omega_{ax0}) + \cos \theta (J_{exx} - J_{eyy}) (\omega_{ax0})$$

$$g_{z2} = g_{z4} = 2 \tan \theta (J_{exx} + J_{azz}) (\omega_{ay0}) - K_{af}$$

The exogenous disturbance  $w$  is time varying and satisfies the constraint in a fixed finite time interval

$$\int_0^T w^T(t) w(t) dt \leq d^2, d \geq 0 \quad (35)$$

### 3. Controller design in finite time application occasions

We need the following FTB concept for LPV system. Given a positive scalar  $T$  and a class of exogenous disturbance signals  $w$  defined as (35), the closed-loop system

$$\dot{x}(t) = A(p(t))x(t) + B(p(t))u(t) + G(p(t))w(t) \quad (36)$$

is said to be finite-time bounded with respect to  $(c_1, c_2, T, R, d)$  ( $c_1 < c_2$  and  $R > 0$ ), if

$$x^T(0)Rx(0) \leq c_1^2 \Rightarrow x^T(t)Rx(t) \leq c_2^2, \quad (37)$$

$$\forall t \in [0, T], \forall w : \int_0^T w^T(t) w(t) dt \leq d^2, d \geq 0$$

Given system(36), there exists a state feedback in form of  $u(t) = K(p(t))x(t)$  such that the system

$$\dot{x}(t) = (A(p(t)) + K(p(t)))x(t) + G(p(t))w(t) \quad (38)$$

is FTB if, fix a scalar  $\alpha \geq 0$  and find two symmetric positive definite matrices  $Q_1 \in R^{n \times n}$  and  $Q_2 \in R^{l \times l}$  and matrices  $L_j \in R^{m \times n}$ ,  $j = 1, \dots, N$ , and positive scalars  $\lambda_1, \lambda_2, \lambda_3$  such that the following LMIs hold

$$\lambda_1 I < Q_1 < I \quad (39)$$

$$\lambda_2 I < Q_2 < \lambda_3 I \quad (40)$$

$$\begin{bmatrix} c_2^2 e^{-\alpha T} & c_1 & d \\ c_1 & \lambda_1 & 0 \\ d & 0 & \lambda_2 \end{bmatrix} > 0 \quad (41)$$

**Table 1**

The gimbal parameters assumed in the simulation.

	Inner	Outer
Axis	$J_{lx} = 0.05 \text{ kg m}^2$	$J_{ox} = 0.1 \text{ kg m}^2$
Iner-tia	$J_{ly} = 0.325 \text{ kg m}^2$	$J_{oy} = 0.4 \text{ kg m}^2$
	$J_{lz} = 0.2 \text{ kg m}^2$	$J_{oz} = 0.6 \text{ kg m}^2$
Axis viscous Friction	$K_{if} = 0.56 \text{ kg m/rad/s}$	$K_{of} = 0.56 \text{ kg m/rad/s}$
Axis Coulomb Friction	$T_{I,fric} = 0.75 \text{ kg m/rad/s}$	$T_{O,fric} = 0.75 \text{ kg m/rad/s}$
Axis cable restraint	$K_{lo} = 0.1 \text{ kg m/rad}$	$K_{Oo} = 0.1 \text{ kg m/rad}$

$$\Theta_{ij} + \Theta_{ji} < 0, 1 \leq i < j \leq N \quad (42)$$

$$\Theta_{ii} < 0, i = 1, \dots, N \quad (43)$$

where

$$\Theta_{ij} = \begin{bmatrix} M & G_i Q_2 \\ Q_2 G_i^T & -Q_2 \end{bmatrix}, 1 \leq i, j \leq N \quad (44)$$

$$M = A_i R^{-\frac{1}{2}} Q_1 R^{-\frac{1}{2}} + B_i L_j + \left( A_i R^{-\frac{1}{2}} Q_1 R^{-\frac{1}{2}} + B_i L_j \right)^T - \alpha R^{-\frac{1}{2}} Q_1 R^{-\frac{1}{2}} \quad (45)$$

then the state feedback gain is given by

$$K(p) = \sum_{j=1}^N p_j(t) K_j, \sum_{j=1}^N p_j(t) = 1, p_j(t) \geq 0, j = 1, \dots, N \quad (46)$$

with

$$K_j = L_j \left( R^{-\frac{1}{2}} Q_1 R^{-\frac{1}{2}} \right)^{-1} \quad (47)$$

**Remark:** In order to solve the controller design problem with the sufficient conditions above, we need to use the LMI toolbox to solve LMI feasibility problem, which is described by conditions (39)–(45), then evaluate the state feedback matrix  $K_j$ . The detailed proof of the sufficient condition is shown in reference [23]. However, we solve LMI feasibility problem to get a controller, instead of minimize linear objective under LMI constraints in [23].

The principle of parameter setting should be determined before designing the controller. Design specifications of the controller depends on the stability requirement, the intensity of the movement of the base and the sensor specifications. When the lead-proportional-integral controller is adopted in the single-channel decoupling model, P. Garnell [24] illustrated how to determine the design specifications and how to compromise in a given condition. However, with the controller design method presented in this paper, the controller parameters depend on  $c_1, c_2, T, d$ . The desired finite time  $T$ , scalar  $\alpha$  and the ratio of  $c_1$  and  $d$  is determined by the typical working mode. The value of  $c_2$  will have an effect on the specifications of the two-axis gimbal platform, such as bandwidth and settling time. A smaller  $c_2$  will result in a bigger gain and a higher bandwidth. When an application environment is determined ( $c_1, \alpha, T, d$  is determined), the design process can be simplified as adjusting  $c_2$ .

The controller is designed with the following gimbal parameters, which were listed in Table 1.

Considering a typical application environment,  $c_1, c_2$ , and  $d$  is set as  $c_1 = 1, c_2 = 165, T = 13$  and  $d = 1$ . At the same time, limited working time is set to 13 s. The LMI feasibility problem yields the state feedback matrix with

$$K_1 = \begin{bmatrix} -0.0396 & -68.3903 & -0.001 & 0.0290 \\ -0.003 & 0.0118 & -0.0967 & -132.5956 \end{bmatrix}, \quad K_2 = \begin{bmatrix} -0.0396 & -68.3903 & 0.001 & -0.0290 \\ 0.003 & -0.0118 & -0.0967 & -132.5956 \end{bmatrix}, \quad (48)$$

$$K_3 = \begin{bmatrix} -0.0396 & -28.8318 & -0.001 & 0.0290 \\ -0.003 & 0.0118 & -0.0967 & -35.2223 \end{bmatrix}, \quad K_4 = \begin{bmatrix} -0.0396 & -28.8318 & 0.001 & -0.0290 \\ 0.003 & -0.0118 & -0.0967 & -35.2223 \end{bmatrix}$$

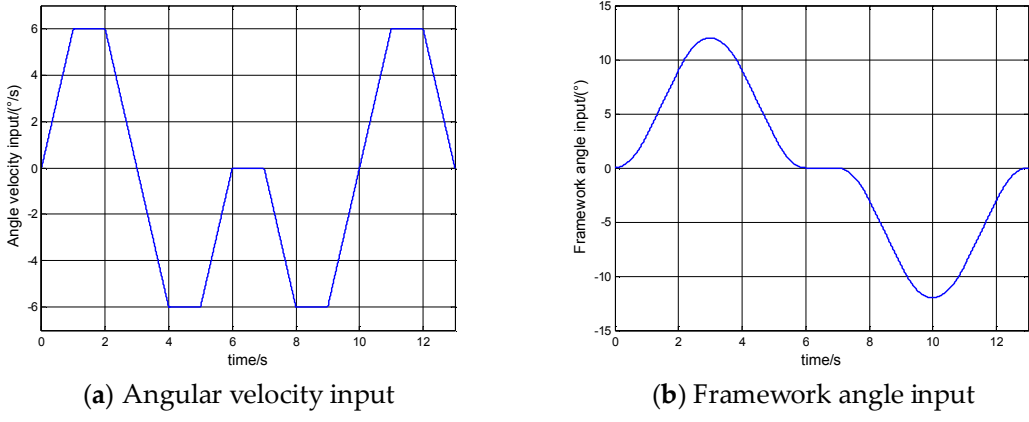


**Fig. 3.** Angular velocity and framework angle input.

The state feedback gain is given by(46), with

$$p_1 = \frac{(0.5 - \omega_{ax}) + (0.5 - \omega_{ay})}{4} \quad (49)$$

$$p_2 = \frac{(0.5 - \omega_{ax}) + (0.5 + \omega_{ay})}{4} \quad (50)$$

$$p_3 = \frac{(0.5 + \omega_{ax}) + (0.5 - \omega_{ay})}{4} \quad (51)$$

$$p_4 = \frac{(0.5 + \omega_{ax}) + (0.5 + \omega_{ay})}{4} \quad (52)$$

According to (3), we can get  $\omega_{ax}$  and  $\omega_{ay}$  by the angular velocity of the base, which is measured by the gyroscopic mounted on the base.

$$\omega_{ax} = p \cos \psi + q \sin \psi \quad (53)$$

$$\omega_{ay} = -p \sin \psi + q \cos \psi \quad (54)$$

#### **4. Simulation and results**

The two-axis gimbal platform was simulated in order to provide a comparison of the controller designed in this paper and a PI compensator. Two rate gyros are chosen to provide angular velocity information of the gimbal in the control process, whose constant drift is  $15^\circ/\text{h}$ . A PI compensator was given by

$$G_c(s) = 18 \frac{s+25}{s} \quad (55)$$

In order to test the designed FTB controller performance in a limited time, especially the pitch and yaw channel coupling interference suppression performance, a simulation experiment is designed. The sinusoidal disturbance rates are  $p = q = r = 3 \sin(6\pi)$ . The simulation represents a typical disturbance environment with aircraft. System input angular velocity is section of trapezoidal wave, the maximum angular velocity is  $6^\circ/\text{s}$ . Angular velocity input and the corresponding framework angle input is shown in Fig. 3.

When the pitch channel tracking the input signals, pitch output error and yaw coupling error are shown in Fig. 4(a) and (b). Even if the input is a single frequency sine signals, yaw channel also can produce error due to the coupling. It can be seen from the diagram that, the max tracking error of pitch channel were  $0.2^\circ/\text{s}$  with both PI and FTB controller. The max coupling error of yaw channel with PI controller is  $0.8^\circ/\text{s}$ , however, the max coupling error of yaw channel with FTB controller is down to  $0.2^\circ/\text{s}$ .

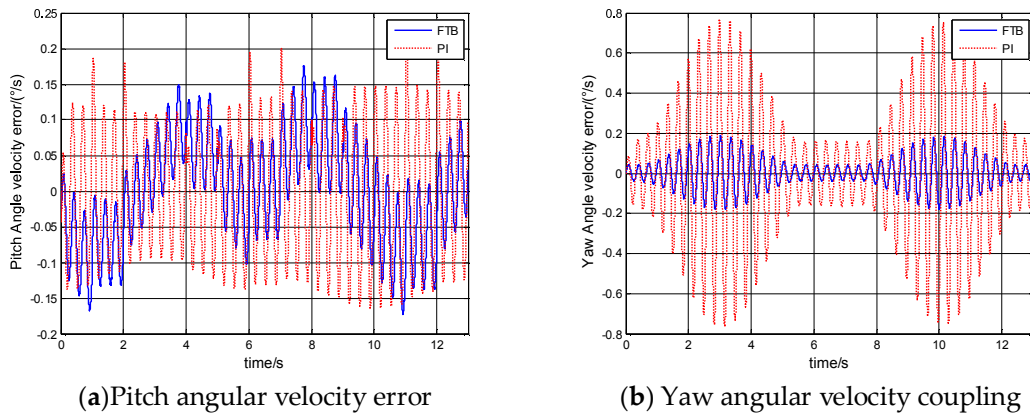


Fig. 4. Angular velocity output when pitch channel tracking orders.

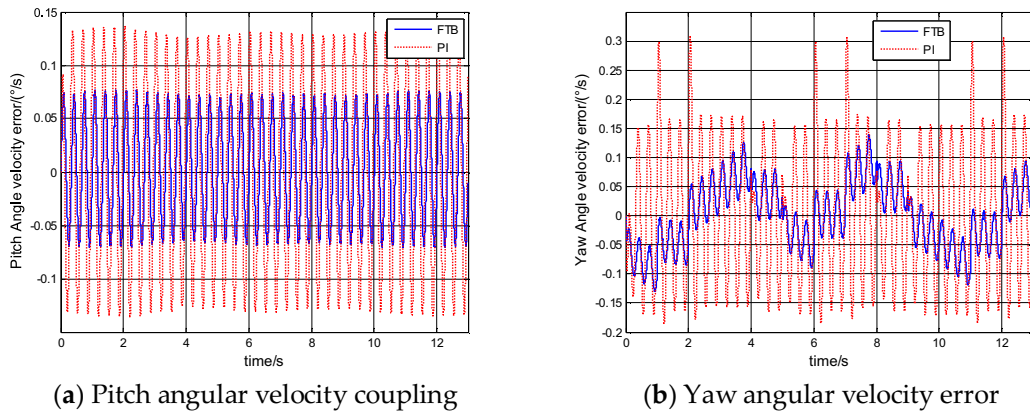


Fig. 5. Angular velocity output when yaw channel tracking orders.

**Table 2**

Error analysis results of elevation and azimuth channels.

	Pitch channel error		Yaw channel error	
	PI controller	FTB controller	PI controller	FTB controller
IAE	0.01881	0.01417	0.02393	0.01086
ISE	3.507e-5	2.304e-5	5.9e-5	1.321e-5

When the yaw channel tracking the input signals, pitch coupling error and yaw output error are shown in Fig. 5(a) and (b). It can be seen that the max tracking error in yaw channel with PI controller is  $0.3^{\circ}/s$  and that with FTB controller is down to  $0.14^{\circ}/s$ . As for the max coupling error, FTB controller reduced that from  $0.14^{\circ}/s$  to  $0.06^{\circ}/s$ .

In order to support the performance analysis, a quantitative study of error analysis has been achieved utilizing two frequently used error integral criteria; integral square error(ISE) and integral absolute error(IAE):

$$\begin{aligned} ISE &= \int_0^T |e(t)|^2 dt \\ IAE &= \int_0^T |e(t)| dt \end{aligned} \quad (56)$$

where  $e(t)$  is the measured error, and  $T = 13$ . The values of error integral criteria obtained for elevation and azimuth channels are provided in Table 2, which indicates that the error in FTB controller is minimum as compared to PI controller which shows the superiority of the proposed FTB controller.

To quantitative coupling error between pitch and yaw channel, we statistic the coupling output in 13 s. That is to say, we cumulative the pitch angular velocity coupling when yaw channel tracking orders and the yaw angular velocity coupling when pitch channel tracking orders. We also use the ISE and IAE to measure coupling. The quantitative results are provided

**Table 3**

coupling interference analysis results of elevation and azimuth channels.

Yaw channel coupling		Pitch channel coupling	
	PI controller		FTB controller
IAE	0.05914	0.0143	0.01882
ISE	4.3e-4	2.524e-5	3.371e-5

in Table 3. It can be seen from the table that, compared to PI controller, FTB controller have a stronger coupling inhibition ability.

## 5. Conclusions

In this paper, we developed the dynamic model of a pitch-yaw gimbal platform and presented its LPV form. A FTB controller is proposed to improve the performance under disturbance in finite time. A simulation test was designed to compare the controller presented in the paper and the PI controller. The results show that the FTB controller has a stronger disturbance rejection and coupling inhibition capability. The design and analysis method can be applied in the controller design of seeker or some other pitch-yaw gimbaled sensor system.

## Conflicts of interest

The authors declare that there is no conflict of interests regarding the publication of this article.

## Author contributions

Yang Chen conceived the methodology and wrote the paper. Hairong Chu and Lihong Guo designed and performed the experiment. Tingting Sun and Feng Zhang developed the program used in the experiment.

## Acknowledgments

None.

## References

- [1] Y. Zhang, C. Du, Q. Mu, Random error modelling and compensation of accelerometer in airborne remote sensing stabilized platform, *Trans.- Inst. Meas. Control* 35 (4) (2013) 503–509.
- [2] L.I. Jia-Quan, C. Ding, D.J. Kong, et al., Velocity based disturbance observer and its application to photoelectric stabilized platform, *Opt. Precis. Eng.* 19 (5) (2011) 998–1004.
- [3] B. Ekstrand, Equations of motion for a two-axes gimbal system, *IEEE Trans. Aerosp. Electron. Syst.* 37 (3) (2001) 1083–1091.
- [4] M.M. Abdo, A.R. Vali, A.R. Toloei, et al., Improving two axes gimbal seeker performance using cascade control approach, *Proc. Inst. Mech. Eng. Part G: J. Aerosp. Eng.* 229 (1) (2015) 38–55.
- [5] P.J. Kennedy, R.L. Kennedy, Direct versus indirect line of sight (LOS) stabilization, *IEEE Trans. Control. Syst. Technol.* 11 (1) (2003) 3–15.
- [6] K. Bansal, L. Dewan, Comparison of different controllers for line-of-sight stabilization of a gimbal systemEngineering and systems, *IEEE* (2014) 1–5.
- [7] W. Ji, Q. Li, B. Xu, et al., Adaptive fuzzy PID composite control with hysteresis-band switching for line of sight stabilization servo system, *Aerospace Sci. Technol.* 15 (1) (2011) 25–32.
- [8] M.M. Abdo, A.R. Vali, A.R. Toloei, et al., Stabilization loop of a two axes gimbal system using self-tuning PID type fuzzy controller, *ISA Trans.* 53 (2) (2014) 591–602.
- [9] S.B. Kim, S.H. Kim, Y.K. Kwak, Robust control for a two-axis gimbaled sensor system with multivariable feedback systems, *IET Control Theory Appl.* 4 (4) (2010) 539–551.
- [10] Z. Liu, Q. Bao, Y. Xia, et al., H-infinity mix sensitivity controller design based on GIMC for electro-optical stabilization and tracking system, in: *International Symposium on Photoelectronic Detection & Imaging*. International Society for Optics and Photonics, 2013, 89061Y-89061Y-10.
- [11] S. Iqbal, A.I. Bhatti, M. Akhtar, et al., Design and robustness evaluation of an  $H_{\infty}$  loop shaping controller for a 2DOF stabilized platform, *IEEE, Control Conference* (2015) 2098–2104.
- [12] B.J. Smith, W.J. Schrenk, W.B. Gass, et al., Sliding mode control in a two-axis gimbal system, *IEEE, Aerospace Conference*, 1999. Proceedings 5 (1999) 457–470.
- [13] F.J. Lin, P.H. Shen, Robust fuzzy neural network sliding-mode control for two-axis motion control system, *IEEE Trans. Ind. Electron.* 53 (4) (2006) 1209–1225.
- [14] Y. Zou, X. Lei, A compound control method based on the adaptive neural network and sliding mode control for inertial stable platform, *Neurocomputing* 155 (C) (2015) 286–294.
- [15] A. Naderolasli, M. Tabatabaei, Stabilization of the two-axis gimbal system based on an adaptive fractional-order sliding-mode controller, *IETE J. Res.* 63 (1) (2017) 124–133.
- [16] J.A.R. Krishna Moorthy, Rajeev Marathe, Hari Babu, Fuzzy controller for line-of-sight stabilization systems, *Opt. Eng.* 43 (6) (2004) 1394–1400, Jun 01.
- [17] F. Liu, H. Wang, Fuzzy PID controller for optoelectronic stabilization platform with two-axis and two-frame, *Optik - Int. J. For. Light Electron Opt.* 140 (2017).
- [18] F.F.M. L El-Sousy, K.A. Abuhasel, Adaptive nonlinear disturbance observer using double loop self-organizing recurrent wavelet-neural-network for two-axis motion control system, *IEEE Trans. Ind. Appl.* (99) (2017), 1–1.
- [19] S.P. Bhat, D.S. Bernstein, *Finite-Time Stability of Continuous Autonomous Systems*, Society for Industrial and Applied Mathematics, 2000.
- [20] X. Lin, K. Liang, H. Li, et al., Finite-time stability and stabilization for continuous systems with additive time-varying delays, *Circ. Syst. Signal. Process.* 36 (7) (2017) 2971–2990.

- [21] Z. Zhang, Z. Zhang, H. Zhang, et al., Finite-time stability analysis and stabilization for linear discrete-time system with time-varying delay, *J. Franklin Inst.* 351 (6) (2014) 3457–3476.
- [22] F. Amato, M. Ariola, P. Dorato, Finite-time control of linear systems subject to parametric uncertainties and disturbances, *Automatica* 37 (9) (2001) 1459–1463.
- [23] Y. Shen, Finite-time control of linear parameter-varying systems with norm-bounded exogenous disturbance, *J. Control Theory Appl.* 6 (2) (2008) 184–188.
- [24] P. Garnell, D.J. East, *Guided Weapon Control Systems*, vol. 3, Pergamon press, New York, 1980, pp. 154–196.